CIRP Annals - Manufacturing Technology 00 (2026) 1–5

Contents lists available at ScienceDirect

CIRP Annals - Manufacturing Technology

journal homepage: https://www.editorialmanager.com/CIRP/default.aspx

Assessment of local microscale residual stresses induced by variable uncut chip thickness in turning using large-field FIB-DIC

Gorka Ortiz-de-Zarate (3)[a,*], Andrey Chuvilin[b,c], François Ducobu (2)[d], Aitor Madariaga[a], Mikel Etxebeste[a], Pedro J. Arrazola (1)[a]

[a] Mondragon Unibertsitatea, Faculty of Engineering, Arrasate-Mondragón 20500, Spain
[b] CIC NanoGUNE BRTA, San Sebastian 20018, Spain
[c] Basque Foundation of Science IKERBASQUE, Bilbao 48013, Spain
[d] Machine Design and Production Engineering Lab, Research Institute for Science and Material Engineering, Mons, UMONS, 7000, Belgium

ARTICLE INFO

Article history:
Available online xxx

Keywords:
Residual stress
Surface integrity
Turning
FIB-DIC

ABSTRACT

Variable uncut chip thickness in turning induces spatially heterogeneous thermomechanical loadings that strongly affect residual stress (RS) generation. Conventional techniques, such as laboratory X-ray diffraction (XRD), provide spatially averaged RS values over millimetre-scale areas and cannot resolve local surface RS gradients. This work introduces a large-field Focused Ion Beam-Digital Image Correlation (FIB-DIC) methodology using slits and ring-cores to quantify local microscale RS, combined with stereo profilometry to correlate stresses with surface topography in turned Ti-6Al-4V ELI. The results reveal peak-to-valley RS variations up to 1000 MPa, undetectable by XRD, highlighting their potential impact on fatigue, corrosion, and surface-driven component performance.

1. Introduction

Turning is extensively used to manufacture critical components for aerospace, biomedical, and automotive sectors, where stringent surface integrity (SI) requirements must be met [1–5]. Among SI parameters, residual stresses (RS) and surface topography are especially critical, as tensile RS and increased roughness deteriorate fatigue and corrosion performance [6–8].

During turning, the final surface is generated by successive tool revolutions, and the finite tool corner radius causes the uncut chip thickness to vary continuously along the cutting edge. These conditions lead to: i) repeated thermomechanical loading by successive tool revolutions, which modifies the stress state imposed from the preceding revolution; and ii) non-uniform strain and temperature fields arising from local variations in uncut chip thickness [9–12]. Experimental studies have linked these mechanisms to heterogeneous hardness and white-layer formation [9], while numerical works have predicted strongly heterogeneous RS fields, often exhibiting periodic patterns correlated with surface topography [10–12].

Despite these advances, experimental validation of local RS heterogeneity in turning remains scarce. This is primarily due to the spatial averaging inherent in conventional RS measurement techniques. Laboratory X-ray diffraction (XRD) and hole-drilling methods probe areas defined by the collimator or milling tool diameter, typically ranging from several hundreds of micrometres to millimetres [13,14]. As a result, local RS variations are averaged out, hindering direct correlation between RS, surface topography, and functional performance.

High-spatial-resolution techniques are thus required to resolve local RS variations in machined surfaces. The combination of Focused Ion Beam (FIB) milling and Digital Image Correlation (DIC) provides high-fidelity local RS measurement with micrometric spatial resolution by coupling controlled material removal with nanoscale deformation mapping [15]. FIB-DIC has been successfully applied to coatings [16,17], peened surfaces [18], additively manufactured materials [19], and, to a limited extent, machining processes (orthogonal cutting [20] and milling [21]). These studies revealed pronounced local stress concentrations and stress sign reversals in high deformation processes that cannot be captured by XRD [18–21]. Although FIB-DIC can characterise RS at the micrometric scale, it has not yet been systematically applied to investigate the spatially varying RS induced by variable uncut chip thickness and successive tool revolutions in turning. This approach would improve analysis of fatigue and corrosion failure mechanisms and support the development of more accurate predictive models.

This work employs large-field FIB-DIC to quantify local microscale RS and, combined with SEM stereo profiling, to correlate RS with surface topography in turned samples. FIB-milled slits and ring-cores with nano-DIC provide high-fidelity RS data in the cutting direction over extended surface regions, while in-plane RS components are obtained at selected locations. XRD measurements are used for comparison. The method is applied to the widely used biomedical alloy Ti-6Al-4V ELI at varying cutting speeds to generate distinct SI and RS states. This allows direct assessment of the effect of variable uncut chip thickness on local RS distributions and their correlation with surface topography.

2. Methodology

2.1. Turning tests

Turning tests were conducted on Ti-6Al-4V ELI (chemical composition in Table 1). A cylindrical bar (Ø113 mm) was annealed at 720 °C for 2 h and furnace-cooled, resulting in a hardness of 320 ± 15 HV. The initial microstructure consisted of primary α-phase grains (≈12 μm),

* Corresponding author.
E-mail address: gortizdezarate@mondragon.edu (G. Ortiz-de-Zarate).

https://doi.org/10.1016/j.cirp.2026.04.070

Table 1
Chemical composition (wt. %) of Ti-6Al-4V ELI.

C (%)	Fe (%)	O (%)	N (%)	V (%)	Al (%)	Ti (%)
0.02	0.15	0.13	0.0024	3.9	6.22	Bal

β-phase along grain boundaries, and transformed β grains with lamellar secondary α-phase precipitates ($\approx$1 μm).

Turning experiments were conducted on a CNC lathe Danumerik 2 equipped with a Kistler 9121 dynamometer. Force signals were low-pass filtered at 20% of the natural frequency of the system, as recommended by the manufacturer. Preliminary experiments varying cutting speed (v_c), feed (f), and corner radius (r_ε) identified v_c as the most efficient parameter for modifying RS state. Accordingly, v_c was varied from 60 to 600 m/min—exceeding typical industrial values—to induce a range of thermomechanical loads and generate both compressive and tensile RS states for FIB-DIC validation. For each condition, longitudinal turning was conducted over a 15 mm axial length. All other process parameters were kept constant: feed (f = 0.1 mm/rev), depth of cut (a_p = 0.5 mm), and tool (coated cemented carbide insert CNMG 120404-QM 1205, r_ε = 0.4 mm). The resulting uncut chip thickness at the machined surface ranged from 0 to 0.025 mm. High-pressure coolant (100 bar, Vasco 7000, 8% emulsion) was applied through the toolholder (QS-PCLNL 2020-12C). The cutting edge radius of all tools was measured using an Alicona IFG6 (10× magnification, 3 μm lateral and 200 nm vertical resolutions) and was of 35 ± 5 μm. A new insert was used for each test, and tool wear was evaluated after each turning test.

2.2. Surface integrity characterisation

Surface profiles and local microscale RS were measured using a Helios 450S FIB/SEM. For each machining condition, 15 × 20 × 9 mm samples were extracted from the turned bar by wire electrical discharge machining. In SEM/FIB the area of interest (170 μm horizontal field of view, larger than the feed marks) was marked by FIB-milled reference crosses (Fig. 1a, b) and imaged at −3°, 0° and +3° tilt angles. Surface topography was reconstructed from the ±3° stereo images [22] (Fig. 1c, d), and the 0° image was used as the reference for strain analysis.

Slits (150 × 5 × 8 μm, L × W × D) oriented perpendicular to the cutting direction (Fig. 1e), and ring-core features (12 μm inner diameter, 8 μm depth; Fig. 1f) were FIB-milled within the marked area. The surface was pre-coated with Au nanoparticles (inset in Fig. 1f) and RS relaxation caused by material removal was quantified by high-fidelity DIC [23]. At least three slits were milled on each surface, together with several ring-core features distributed along the machined surface (Fig. 1f).

For the slit geometry, relaxation is constrained in the horizontal/feed direction; therefore, only the vertical/cutting displacement component was considered to characterise the continuous strain distribution along the slit (Fig. 1g). As quantitative RS in slit geometry requires calibration [15], ring-cores were combined with slits to calibrate and determine RS without the need for intensive finite element analysis. The ring-core size was selected to ensure near-complete stress relaxation within the analysed volume [15,17], while maintaining measurement stability and spatial resolution. This provided quantitative evaluation of the in-plane RS tensor averaged over the inner-circle area (Fig. 1h–j). It also reduced sensitivity to grain-scale variability and supported detection of RS variations along the machined surface. RS values at topography peaks and valleys (Fig. 1c, d) were used to convert the strain relief measured in the slits into RS. Assuming a non-equiaxial stress state [18], RS in the cutting ($\sigma_{RS,cutting}$) and feed ($\sigma_{RS,feed}$) directions were calculated using eqs. (1) and 2, respectively. Young's modulus (E = 105 GPa), and Poisson's ratio (ν = 0.32) for Ti-6Al-4V ELI were obtained from ASTM E8 tensile tests. $\Delta\varepsilon_{cutting}$ and $\Delta\varepsilon_{feed}$ are the components of the relieved strain tensor from ring-core DIC in the cutting (Fig. 1h) and feed (Fig. 1i) directions.

$$\sigma_{RS,cutting} = -\frac{E}{1-\nu^2}\left(\Delta\varepsilon_{cutting} + \nu\Delta\varepsilon_{feed}\right) \quad (1)$$

$$\sigma_{RS,feed} = -\frac{E}{1-\nu^2}\left(\Delta\varepsilon_{feed} + \nu\Delta\varepsilon_{cutting}\right) \quad (2)$$

Surface RS were measured by XRD to select two cutting speeds that generate distinct SI conditions and to compare with the FIB-DIC method.

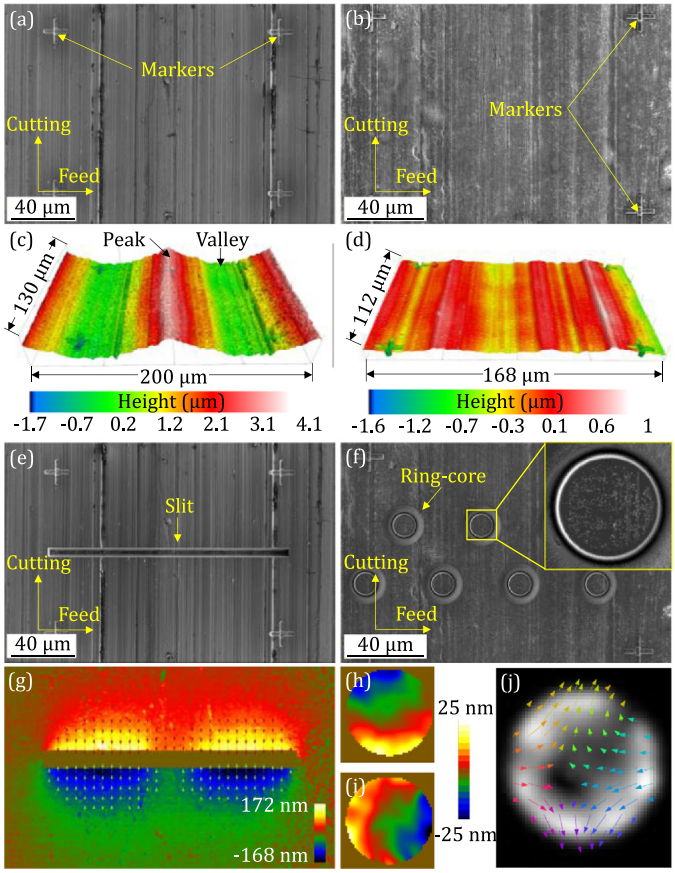

Fig. 1. Workflow for surface topography and RS analysis: (a, b) areas of interest marked by milled crosses at the corners, (c, d) surface topography, (e, f) FIB-milled slit (e) and ring-cores (f), (g) slit-based displacement map by DIC, (h, i) displacement maps in the cutting (h) and feed (i) directions for the ring-core, and (j) displacement vectors obtained from (h, i) overlaid on the displacement amplitude map. (a, c, e, g) correspond to v_c = 60 m/min, and (b, d, f, h–j) to v_c = 600 m/min.

A portable Proto iXRD system was used with the $\sin^2\psi$ method, Cu Kα radiation (λ = 1.5418 Å), Ni filters, 25 kV voltage, 5 mA current, and a Ø3 mm round collimator. The (213) diffraction peak was acquired with 11 tilt angles from −27° to 27° and 20 exposures of 4 s per tilt. Data was analysed using PROTO XrdWin software, applying diffraction elastic constants $-S_1 = 2.97\times10^{-6}$ MPa^{-1}, $^1/_2\,S_2 = 11.89\times10^{-6}$ MPa^{-1}. A Gaussian fit was applied. Measurements were first taken at three circumferential locations separated by 120° on the bar surface to assess repeatability, and subsequently on sectioned specimens prepared for FIB-DIC to evaluate the effect of the sectioning operation (Fig. 2a).

Finally, subsurface microstructural damage was assessed in cross-section using a Nova NanoSEM 450, after cutting, mounting, grinding, polishing, and chemically etching the samples.

3. Results

3.1. Residual stresses by XRD and microstructural damage

Table 2 shows the evolution of surface $\sigma_{RS,cutting}$ measured by XRD. At 60 m/min, RS were strongly compressive, gradually decreasing in magnitude as cutting speed increased, and approaching a near-neutral or slightly tensile state at 600 m/min. For this reason, cutting speeds of 60 and 600 m/min were selected for validation of the FIB-DIC method.

Table 2
$\sigma_{RS,cutting}$ with cutting speed measured by XRD on the bar.

Cutting speed (m/min)	60	200	400	600
$\sigma_{RS,cutting}$ (MPa)	−559 ± 20	−414 ± 22	−100 ± 32	9 ± 38

Fig. 2a presents the repeatability analysis for RS measured by XRD in the cutting and feed directions (solid bars). Deviations among the three measurement points remained below 40 MPa. The figure also shows the effect of specimen sectioning prior to FIB-DIC analysis, with

Please cite this article as: G. Ortiz-de-Zarate et al., Assessment of local microscale residual stresses induced by variable uncut chip thickness in turning using large-field FIB-DIC, CIRP Annals - Manufacturing Technology (2026), https://doi.org/10.1016/j.cirp.2026.04.070

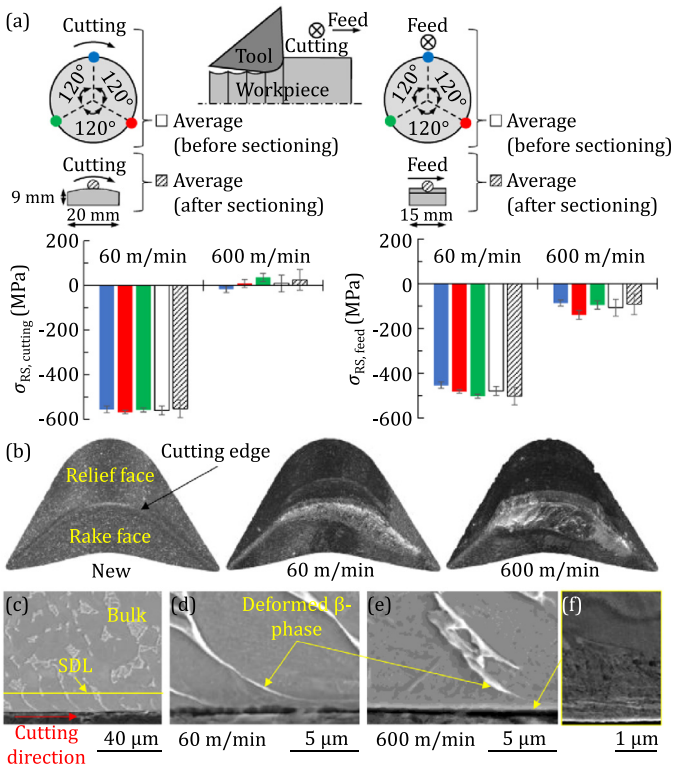

Fig. 2. (a) $\sigma_{RS,cutting}$ and $\sigma_{RS,feed}$ measured by XRD, (b) tool geometry before and after turning, (c) surface micrograph after machining at v_c = 60 m/min, (d, e) detailed micrographs of the severely deformed layer (SDL) at (d) v_c = 60 m/min and (e, f) v_c = 600 m/min, and (f) detailed micrograph of the recrystallised zone.

empty bars representing the average RS of the three points before sectioning and striped bars after. The maximum difference between mean surface RS values before and after sectioning was below 25 MPa, i.e., within experimental uncertainty, indicating that sectioning did not significantly affect the RS state. For consistency, post-sectioning RS values are used for comparison with FIB-DIC results.

After sectioning, the RS in the cutting direction were highly compressive at v_c = 60 m/min (−551 ± 39 MPa) and shifted to slightly tensile at v_c = 600 m/min (24 ± 47 MPa). A similar trend was observed in the feed direction, with strongly compressive stresses at v_c = 60 m/min (−503 ± 40 MPa) and lower-magnitude compressive stresses at v_c = 600 m/min (−91 ± 35 MPa).

At low cutting speed, the relatively low thermal input combined with high contact pressures at the tool-workpiece interface promoted plastic deformation in the near-surface layer, resulting in compressive RS. As cutting speed increased, RS progressively shifted toward tensile in both directions, driven by higher thermal loading and reduced mechanical contribution [24], as reflected in the measured forces. At v_c = 60 m/min, the cutting, feed, and passive forces were F_c = 135 ± 5 N, F_f = 112 ± 2 N, and F_p = 70 ± 2 N, respectively. At v_c = 600 m/min, these forces decreased to F_c = 121 ± 3 N, F_f = 57 ± 3 N, and F_p = 43 ± 3 N. Elevated temperatures at higher speeds induced local thermal softening and reduced chip thickness [25], thereby lowering the cutting forces.

At v_c = 600 m/min, tool wear further reduced forces. The cutting edge radius decreased from ≈35 µm to ≈10 µm as flank wear (maximum $V_{B,max}$ ≈ 0.15 mm, average $V_{B,mean}$ ≈ 0.08 mm) sharpened the edge, reducing ploughing force. At the same time, crater wear (depth K_T ≈ 25 µm, width K_B ≈ 0.25 mm) increased the local rake angle, facilitating chip flow and further reducing forces (Fig. 2b). In contrast at v_c = 60 m/min, wear was minimal: only slight material adhesion occurred on the rake face, and the edge radius remained near the initial ≈35 µm.

Microstructural analysis revealed three distinct zones (Fig. 2c–f): i) bulk material, ii) a plastically deformed subsurface layer with grains elongated in the cutting direction (surface drag), and iii) thinning and elongation of the β-phase in the cutting direction (Fig. 2d, e). The thickness of the severely deformed layer (SDL) increased with cutting speed, from ≈12 µm at 60 m/min to ≈20 µm at 600 m/min. At v_c = 600 m/min, a recrystallised α-phase was also observed in the topmost zone (Fig. 2f).

Overall, the machining conditions produced well-differentiated RS states and associated microstructural alterations, establishing suitable boundary conditions to assess FIB-DIC measurements across distinct surface integrity regimes.

3.2. Local microscale RS by FIB-DIC and surface topography

Fig. 3 shows the local microscale surface RS measured along the turned surface using the FIB-DIC slitting method for both cutting speeds (left axis), and the corresponding surface topography measured by stereo profilometry at the same locations (red line, right axis). The plot integrates multiple (≥3) translated and realigned measurements and their deviations (shaded regions). Markers connected by dashed lines denote average results from the FIB-DIC ring-core method at selected surface positions. The mean deviation in slits and ring-core measurements, normalised by the material yield stress (793 ± 10 MPa from the tensile tests), is below 10%. XRD values, which inherently represent an average RS over the Ø3 mm round collimator, are shown as horizontal dotted lines. The peak-to-peak average RS measured by FIB-DIC is indicated by horizontal dash-dotted lines. The *X*-axis corresponds to the tool feed movement direction (left to right).

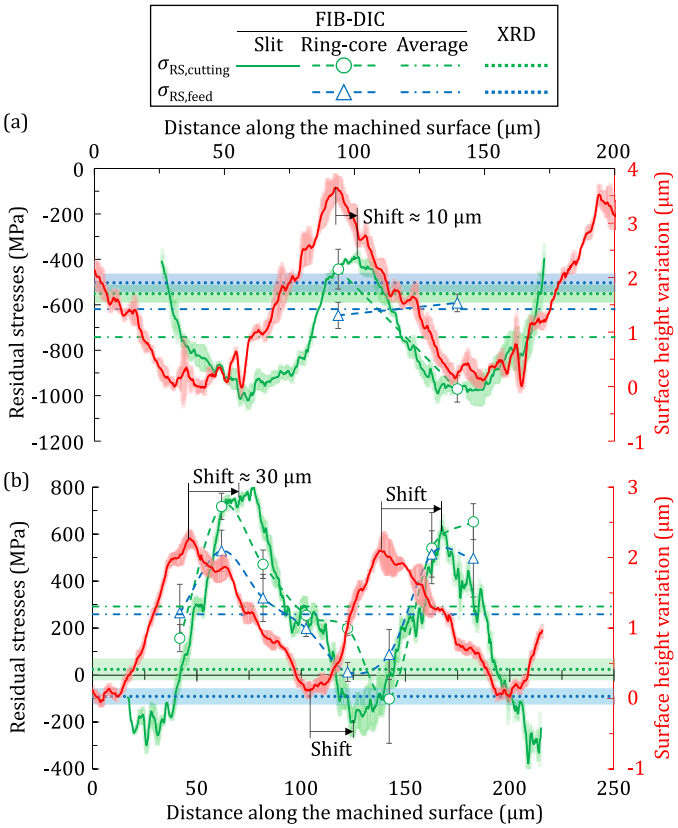

Fig. 3. Local surface RS and surface topography for (a) v_c = 60 m/min and (b) v_c = 600 m/min. Solid lines show mean topography and slit RS, while shaded regions indicate the standard deviation across repetitions.

At v_c = 60 m/min, the most compressive local RS measured by slitting coincides with the valleys of the surface topography (≈−1000 MPa). Peaks exhibit less compressive stresses (≈−400 MPa), resulting in peak-to-valley variations of ≈600 MPa. The high compressive RS at the valleys, which exceeds the yield stress of Ti-6Al-4V ELI, is attributed to localised work-hardening and increased local yield stress. The average RS across the peak-to-peak range measured by FIB-DIC is $\sigma_{RS,cutting}$ ≈ −740 MPa and $\sigma_{RS,feed}$ ≈ −620 MPa. At v_c = 600 m/min, valleys remain the most compressive regions (≈−200 MPa), while highly tensile stresses are observed at the peaks, reaching values of up to ≈800 MPa. Under these conditions, the peak-to-valley RS variation increases markedly to ≈1000 MPa, with average FIB-DIC values of $\sigma_{RS,cutting}$ ≈ 290 MPa and $\sigma_{RS,feed}$ ≈ 260 MPa. The ring-core method reveals that at 600 m/min, substantial RS variations also develop in the feed direction, whereas at 60 m/min, the variation is negligible.

Please cite this article as: G. Ortiz-de-Zarate et al., Assessment of local microscale residual stresses induced by variable uncut chip thickness in turning using large-field FIB-DIC, CIRP Annals - Manufacturing Technology (2026), https://doi.org/10.1016/j.cirp.2026.04.070

A further distinction between the two cutting speeds is the relative spatial shift between topographical features and RS extrema across the machined surface (black arrows, Fig. 3). At 60 m/min, only a small offset (≈10 μm in the tool travel direction) is observed between the RS peaks and the corresponding topographical peaks. In contrast, at 600 m/min a much larger shift (≈30 μm) is evident, with topographical peaks located significantly upstream of the corresponding RS maxima.

4. Discussion

4.1. Comparison between FIB-DIC and XRD for RS analysis

These FIB-DIC results clearly demonstrate that RS shows a periodic pattern and is not homogeneous across the machined surface after turning. In contrast, conventional XRD measurements, characterised by a relatively large beam size, average the RS field over several feed marks, limiting their ability to resolve local microscale and periodic RS variations.

Despite this difference, the average RS values obtained by FIB-DIC along the machined surface agree with the XRD results (Fig. 3), particularly at v_c = 60 m/min, likely due to the lower RS variability. Additionally, both methods exhibit consistent cutting speed trends, indicating that the observed differences are quantitative rather than qualitative.

However, FIB-DIC systematically yields higher RS magnitudes than XRD for both compressive and tensile stress states, likely due to the fundamentally different physical principles of the two methods. XRD predominantly measures macroscopic RS and involves spatial averaging over a finite gauge volume, which smooths steep stress gradients typical of machined surfaces. In contrast, FIB-DIC produces nearly complete microscale local elastic strain release and captures combined macro-, intergranular, and intragranular RS contributions [20], resulting in systematically higher measured RS magnitudes. The effective probing depth of the FIB-DIC features (≈8 μm) also differs slightly from the penetration depth of XRD in titanium alloys (≈5 μm) [26,27], which may contribute to the observed differences.

4.2. Correlation between surface topography and local microscale RS

The combined use of FIB-DIC and stereo profilometry directly correlates local microscale RS and surface topography, providing enhanced insight into surface integrity. FIB-DIC revealed peak-to-valley RS variations of several hundred MPa, not detectable by conventional XRD. The pronounced RS variations along the machined surface are qualitatively consistent with nose-turning finite element method (FEM) predictions reported in the literature [10–12], with quantitative differences attributable to variations in material properties and cutting conditions.

These observations reflect the underlying mechanisms of RS formation. During machining, RS arise from the interplay between mechanical and thermal loads, whose relative contributions depend on the uncut chip thickness, among other factors. In turning, local variations in uncut chip thickness—primarily governed by the tool corner radius and feed—modify the thermomechanical load distribution, as also shown in nose-turning FEM studies [10–12]. Combined with repeated loading from successive tool revolutions, this leads to a non-uniform and periodic RS field along the feed direction of the turned specimens.

At 60 m/min, compressive RS dominate both peaks and valleys, with maximum compression in the valleys, indicating a mainly mechanically driven RS. In contrast, RS in the feed direction remain relatively uniform, reflecting more homogeneous mechanical loading along the tool-workpiece contact.

At 600 m/min, the RS distribution changes substantially: valleys remain mildly compressive, whereas peaks become highly tensile, indicating a transition toward a locally thermally dominated RS generation regime. This trend is intensified by increased flank wear at higher cutting speeds, which enhances heat generation in the tertiary shear zone, modifies heat-flux distribution [24], and promotes larger RS fluctuations in the cutting and feed directions.

FIB-DIC reveals a systematic shift between surface topography extrema and RS extrema in the cutting direction, increasing from ≈10 μm at 60 m/min to ≈30 μm at 600 m/min. This could indicate that RS formation is not instantaneous but continues after tool passage due to delayed thermal diffusion and near-surface strain relaxation, particularly under thermally dominated conditions.

From a functional perspective, the correlation between surface topography and RS is key for assessing component performance, including fatigue and corrosion. Stress concentrations arising from surface topography [7,8] can be significantly amplified by local RS variations, which are often assumed to be spatially uniform in predictive models. These interactions should thus be explicitly considered in high-fidelity performance assessment models.

5. Conclusions

This work demonstrates that the variable uncut chip thickness inherent to turning induces strongly heterogeneous RS fields that cannot be resolved by conventional, spatially averaged techniques. By combining high-fidelity large-field FIB-DIC with stereo profilometry, local microscale RS distributions were measured and directly correlated with surface topography in turned Ti-6Al-4V ELI. Peak-to-valley RS variations of up to 1000 MPa were observed, in sharp contrast to XRD results that provide only average RS.

At low cutting speed (60 m/min), RS generation is predominantly mechanical, leading to pronounced RS fluctuations in the cutting direction, compressive RS across the surface with maximum compression at valleys, and negligible variations in the feed direction. At high cutting speed (600 m/min), a transition to a thermally dominated regime occurs: compressive RS persist in valleys, while highly tensile RS develop at peaks, accompanied by pronounced RS gradients in both the cutting and feed directions. The increasing spatial shift between topography extrema and RS maxima with cutting speed highlights the role of delayed thermal diffusion and post-tool strain relaxation in RS.

These findings confirm that RS in turning are governed by a strong coupling between feed-induced geometric periodicity, local surface topography, and the balance between mechanical and thermal loading. These findings underline the need for high-spatial-resolution techniques, such as large-field FIB-DIC, for realistic surface integrity assessment. They also provide detailed experimental evidence to enhance predictive models for fatigue, corrosion, and surface-driven performance in turned components. While this study focused on a titanium alloy and turning operation, similar RS fluctuations—likely of different magnitude and frequency—could be expected in other materials, cutting conditions, and machining processes with variable uncut chip thickness.

Declaration of competing interest

The authors declare that they have no known competing financial interests or personal relationships that could have appeared to influence the work reported in this paper.

CRediT authorship contribution statement

Gorka Ortiz-de-Zarate: Writing – review & editing, Writing – original draft, Visualization, Validation, Supervision, Project administration, Methodology, Investigation, Formal analysis, Data curation, Conceptualization. **Andrey Chuvilin:** Writing – review & editing, Writing – original draft, Supervision, Software, Resources, Project administration, Methodology, Investigation, Funding acquisition, Formal analysis, Conceptualization. **François Ducobu:** Writing – review & editing, Validation, Supervision, Software, Project administration, Methodology, Formal analysis. **Aitor Madariaga:** Writing – review & editing, Validation, Resources, Methodology, Formal analysis. **Mikel Etxebeste:** Writing – review & editing, Validation, Methodology, Formal analysis, Data curation. **Pedro J. Arrazola:** Writing – review & editing, Supervision, Resources, Project administration, Methodology, Funding acquisition, Formal analysis, Conceptualization.

Acknowledgements

The authors acknowledge funding from TAILORSURF (PID2022-139655OB-I00), DIGISUMAN—HPSC (PID2024-162987OA-I00), nG24 (KK-2024/00001), and Maria de Maeztu Units of Excellence Program (MDM-2016-0618). They also thank Dr. Marek Grzelczak for Au nanoparticle colloids and Erika Domínguez for XRD support.

Please cite this article as: G. Ortiz-de-Zarate et al., Assessment of local microscale residual stresses induced by variable uncut chip thickness in turning using large-field FIB-DIC, CIRP Annals - Manufacturing Technology (2026), https://doi.org/10.1016/j.cirp.2026.04.070

References

[1] M'Saoubi R, Axinte D, Soo SL, Nobel C, Attia H, Kappmeyer G, Engin S, Sim WM (2015) High Performance Cutting of Advanced Aerospace Alloys and Composite Materials. *CIRP Annals* 64(2):557–580.
[2] Ulutan D, Ozel T (2011) Machining Induced Surface Integrity in Titanium and Nickel Alloys: A Review. *International Journal of Machine Tools and Manufacture* 51(3):250–280.
[3] Jawahir IS, Brinksmeier E, M'saoubi R, Aspinwall DK, Outeiro JC, Meyer D, Umbrello D, Jayal AD (2011) Surface Integrity in Material Removal Processes: Recent Advances. *CIRP Annals* 60(2):603–626.
[4] Özel T, Ulutan D (2012) Prediction of Machining Induced Residual Stresses in Turning of Titanium and Nickel Based Alloys With Experiments and Finite Element Simulations. *CIRP Annals* 61(1):547–550.
[5] Sela A, Ortiz-De-Zarate G, Soler D, Germain G, Aristimuño P, Arrazola PJ (2021) Measurement of Plastic Strain and Plastic Strain Rate During Orthogonal Cutting for Ti-6Al-4V. *International Journal of Mechanical Sciences* 198:106397.
[6] Ghiotti A, Bertolini R, Sorgato M, Campagnolo A, Savio E, Bruschi S (2022) Ti6Al4V Titanium Alloy Fatigue Strength After AM-and Machining-Based Process Chains. *CIRP Annals* 71(1):461–464.
[7] Mai PT, Bormann T, Mueller U, Kretzer JP, Gibmeier J (2022) Effect of Surface Topography and Residual Stress on the Taper Connection Stability in Total Hip Arthroplasty. *Journal of the Mechanical Behaviour of Biomedical Materials* 128:105119.
[8] Ortiz-de-Zarate G, Madariaga A, Perez I, Arrazola PJ (2024) Analytical Model to Identify Crack Initiation in Machined Aluminium Parts. *Procedia CIRP* 123:274–279.
[9] Bushlya V, Zhou J, Ståhl JE (2014) Modeling and Experimentation on Multistage Work-Hardening Mechanism in Machining With Nose-Radiused Tools and Its Influence on Machined Subsurface Quality and Tool Wear. *The International Journal of Advanced Manufacturing Technology* 73(1):545–555.
[10] Kortabarria A, Arrazola PJ, Ostolaza K (2013) Multi Revolution Finite Element Model to Predict Machining Induced Residual Stresses in Inconel 718. *Procedia CIRP* 8:111–116.
[11] Mondelin A, Valiorgue F, Rech J, Coret M, Feulvarch E (2012) Hybrid Model for the Prediction of Residual Stresses Induced by 15-5PH Steel Turning. *International Journal of Mechanical Sciences* 58(1):69–85.
[12] Dumas M, Fabre D, Valiorgue F, Kermouche G, Van Robaeys A, Girinon M, Brosse A, Karaouni H, Rech J (2021) 3D Numerical Modelling of Turning-Induced Residual Stresses—A Two-Scale Approach Based on Equivalent Thermo-Mechanical Loadings. *Journal of Materials Processing Technology* 297:117274.
[13] Withers PJ, Turski M, Edwards L, Bouchard PJ, Buttle DJ (2008) Recent Advances in Residual Stress Measurement. *International Journal of Pressure Vessels and Piping* 85(3):118–127.
[14] Brinksmeier E, Cammett JT, König W, Leskovar P, Peters J, Tönshoff HK (1982) Residual Stresses—Measurement and Causes in Machining Processes. *CIRP annals* 31(2):491–510.
[15] Lord J, Cox D, Ratzke A, Sebastiani M, Korsunsky A, Salvati E, Mughal MZ, Bemporad E (2018) A Good Practice Guide for Measuring Residual Stresses Using FIB-DIC. *Measurement Good Practice Guide* : 143.
[16] Sebastiani M, Eberl C, Bemporad E, Pharr GM (2011) Depth-Resolved Residual Stress Analysis of Thin Coatings by a New FIB—DIC Method. *Materials Science and Engineering: A* 528(27):7901–7908.
[17] Korsunsky AM, Sebastiani M, Bemporad E (2010) Residual Stress Evaluation at the Micrometer Scale: Analysis of Thin Coatings by FIB Milling and Digital Image Correlation. *Surface and Coatings Technology* 205(7):2393–2403.
[18] Everaerts J, Song X, Nagarajan B, Korsunsky AM (2018) Evaluation of Macro-and Microscopic Residual Stresses in Laser Shock-Peened Titanium Alloy by FIB-DIC Ring-Core Milling With Different Core Diameters. *Surface and Coatings Technology* 349:719–724.
[19] Song X, Feih S, Zhai W, Sun CN, Li F, Maiti R, Wei J, Yang Y, Oancea V, Brandt LR, Korsunsky AM (2020) Advances in Additive Manufacturing Process Simulation: Residual Stresses and Distortion Predictions in Complex Metallic Components. *Materials Design* 193:108779.
[20] Yue Q, Li Y, Liang C, Wang Y, He Y (2024) Quantitative Evaluation of Residual Stress and Microstructural Effects on the Surface Hardness of Machined Ti-6Al-4 V Alloy With Microscopic Characterization Techniques. *Journal of Materials Processing Technology* 327:118382.
[21] He Y, Yue Q, Li Y, He J, Zhong R (2024) Multiscale Residual Stress and Mechanical Behavior Analysis in Machining of Ti-6Al-4V Alloy With Advanced Microscopic Characterization. *Journal of Manufacturing Processes* 120:568–578.
[22] Boyde A (1973) Quantitative Photogrammetric Analysis and Qualitative Stereoscopic Analysis of SEM Images. *Journal of Microscopy* 98(3):452–471.
[23] Lunt AJ, Korsunsky AM (2015) A Review of Micro-Scale Focused Ion Beam Milling and Digital Image Correlation Analysis for Residual Stress Evaluation and Error Estimation. *Surface and Coatings Technology* 283:373–388.
[24] Liu Y, Xu D, Agmell M, M'Saoubi R, Ahadi A, Stahl J, Zhou J (2021) Numerical and Experimental Investigation of Tool Geometry Effect on Residual Stresses in Orthogonal Machining of Inconel 718. *Simulation Modelling Practice and Theory* 106:102187.
[25] Ortiz-de-Zarate G, Madariaga A, Arrazola PJ, Childs TH (2021) A Novel Methodology to Characterize Tool-Chip Contact in Metal Cutting Using Partially Restricted Contact Length Tools. *CIRP Annals* 70(1):61–64.
[26] Martinez SA, Sathish S, Blodgett MP, Shepard MJ (2003) Residual Stress Distribution on Surface-Treated Ti-6Al-4V by X-Ray Diffraction. *Experimental Mechanics* 43(2):141–147.
[27] Umapathi A, Swaroop S (2019) Measurement of Residual Stresses in Titanium Alloys Using Synchrotron Radiation. *Measurement* 140:518–525.

Please cite this article as: G. Ortiz-de-Zarate et al., Assessment of local microscale residual stresses induced by variable uncut chip thickness in turning using large-field FIB-DIC, CIRP Annals - Manufacturing Technology (2026), https://doi.org/10.1016/j.cirp.2026.04.070